PCCP

Accepted Manuscript

ROYAL SOCIETY OF CHEMISTRY

www.rsc.org/pccp

PCCP

RSCPublishing

ARTICLE

Correlation of intercalation potential with d-electron configurations for cathode compounds of lithium-ion batteries

Cite this: DOI: 10.1039/x0xx00000x

Zhenlian Chen[a], Caixia Zhang[a,b], Zhiyong Zhang[c], and Jun Li[a*] ,

Received 00th January 2012,
Accepted 00th January 2012

DOI: 10.1039/x0xx00000x

www.rsc.org/

The d-electron localization is widely recognized important to transport properties of transition metal compounds, but its role in the energy conversion of intercalation reactions of cathode compounds is still not fully explored. In this work, the correlation of intercalation potential to electron affinity, a key energy term controlling electron intercalation, then to d-electron configuration, is investigated. Firstly, we find that the change of the intercalation potential with respect to the transition metal cations within the same structure class is correlated in an approximately mirror relationship with the electron affinity, based on first-principles calculations on three typical categories of cathode compounds including layered oxides and polyoxyanions Then, by using a new model Hamiltonian based on the crystal-field theory, we reveal that the evolution is governed by the combination of the crystal-field splitting and the on-site d-d exchange interactions. Further, we show that the charge order in solid-solution composites and the compatibility of multi-electron redox steps could be inferred from the energy terms with the d-electron configuration alternations. The findings may be applied to rationally designing new chemistry for the lithium-ion batteries and other metal-ion batteries.

1 Introduction

Although the lithium-ion battery (LIB) technology has made great progress in the past several decades, it has encountered a bottleneck that calls for new cathode material systems designed on the basis of better understandings of the intercalation chemistry for energy conversion.[1-3] The energy conversion by Li intercalation in cathode compounds of LIB is attributed to the electron redox energy and the Madelung potential at Li sites, relating to electron intercalation and Li ion intercalation, respectively.[4, 5] The redox reaction in intercalation compounds depends on the formal valence state alternation of the active cation and its covalent bonding with the nearest-neighbour anions.[6] Thus far, the importance of the latter one, i.e., the p-d bonding interactions, which determines the relative position between itinerant p and localized d electrons, has been well illustrated within the conceptual framework of "d-p pinning", proposed by Goodenough et al..[6, 7] And the understanding of the inductive effect originating from the p-d bonding interactions have provided guidance for high-throughput materials screening, which accelerates the exploration of new materials.[8-10] Whereas the former one, which tightly relates to the d-electron localization, mainly determines the redox activity of the transition metal elements (TMEs) in intercalation process. However, the effects of the interactions, rooting in the d-electron localization such as the correlation interactions among d-electrons and the electrostatic repulsion from the ligand ions to the d-electron, on the electron intercalation of cathode compounds have not been fully explored yet.

The responsibility of the correlation interactions for the insulating behaviour is widely studied for cathode compounds, in which the correlation interactions, especially the on-site Coulomb interactions, open or increase the insulating gap.[11-14] It is also well recognized that density functional theory with Hubbard correction (DFT+U) calculations give values of intercalation voltage that agrees better with experiments than DFT calculations.[12, 14, 15] That indicates the importance of the correlation interactions to the energy conversion in intercalation process. In addition, an interesting d(e_g)-p swapping in the oxidation of $LiFePO_4$, in which the insulating gap changes from the Mott-Hubbard-type of $LiFePO_4$ to the charge-transfer-type of $FePO_4$, has been found by electron energy loss spectroscopy and DFT+U calculations.[16] That manifests a collective change of the band structure of the host by redox rather than simple Fermi-level shifting in the rigid-band model,[17] dominated by the correlation interactions. However, the contributions from the correlation interactions to the energy conversion are still not well identified.

In a recent work, we have proposed an intermediate charged state calculation to separate electron intercalation from ion intercalation and explored the relation between the average voltage and the intercalation energy terms. That calculation indicated that the voltage depends on TMEs and lattice types in different manners.[5] In the present work, we aim to demonstrate systematically the relation between intercalation potential and the d-electron localization in terms of the crystal-field (CF) splitting and the correlation interactions in a more comprehensive way with a broader category of intercalation compounds. Firstly, we demonstrate the relationship between the energy contributions from electron and Li ion intercalations and the voltage by performing first-principles calculations for three categories of cathode materials, including oxides and polyoxyanions. Then we propose a simplified model based on CF theory to demonstrate the quantitative correlation between the d-electron configuration and the electron affinity (EA), and thus the intercalation potential. Furthermore, we propose a few arguments for redox mechanisms in solid-solution TME compounds and multi-electron redox couples from the point of view of the intercalation energy terms and the d-electron configurations. We believe that proper separation of the electron and ion contribution to the intercalation reaction and further insight into the d-electron configuration alternations may benefit the top-down design of new chemistry from consideration of lattice types and substitution of active cations. Similar schemes also can be applied to understand the energy conversion of materials for other metal-ion batteries and catalysts for air-batteries, fuel cells, etc.

2 Computational methodology

DFT+U calculations are performed with the Vienna Ab-initio Simulation Package (VASP)[18, 19] using pseudopotentials following the projector augmented wave (PAW) formalism[20, 21] and the exchange and correlation functionals suggested by Perdew, Burke and Ernzerhof (PBE) [22]. The fully localized limit functional introduced by Liechtenstein[23] is chosen for the double-counting term. The DFT+U calculations with the Hubbard correlation parameters, which are dependent on TMEs, formal valence states and other components in the compounds, obtained by the linear response approach, may give calculated values of average voltage very close to the experimental values.[15, 24] But the aim here is not to provide voltage values extremely exact for each individual compounds but to explore the trend-like determining factor for a family of compounds , then the Coulomb repulsion parameter is set to be 5.0 eV for TMEs in oxides and 4.5 eV in phosphates and silicates, and the exchange parameter is set to be 0.5 eV for all compounds, for simplicity and referenced to the literature.[15, 16, 25] A cutoff energy of 500 eV is used for the plane wave expansion of wave functions. The reciprocal space Monkhorst-Pack k-point mesh interval is about 0.04 $Å^{-1}$. The initial structure for layered oxides is taken with experimental $R\bar{3}m$ $LiCoO_2$,[26] phosphates pnma $LiFePO_4$[27] and silicates $pmn2_1$ Li_2FeSiO_4[28]. The small structural effect on energy calculation such as coming from different polymorphs in silicates, is not considered in this work. Structural relaxations are performed with all forces acting on ions converged to less than 0.01 eV/Å. Only ferromagnetic order is assumed for the initial magnetic configurations as the energy contribution of inter-ionic exchange is relatively small (<0.1 eV/f.u.).

To separately derive the contributions of electron intercalation and ion intercalation, the scheme of first-principles calculations of the charged states, proposed in ref. 5, is followed. In that scheme, the intercalation energy is the summation of three energy terms: the EA E_{ea}, the lithium ion affinity E_{la}, and the structure relaxation energy E_{gr} (the corresponding formalism is shown in Fig. S1). We used the charged state calculations as implemented in VASP to separate Li intercalation into electron and ion intercalations[29]. The corrections for charged state calculations take into account (1) the alignment between the average electrostatic potentials of the charged and unchanged host systems in order to remove the arbitrary constant shift of the energy levels due to the removal of the G=0 term and (2) the effects of periodic charge image interactions that include the first order corrections given by the screened Madelung-like lattice energies of point charges and other higher order mutlipole corrections due to the induced charge densities[30].

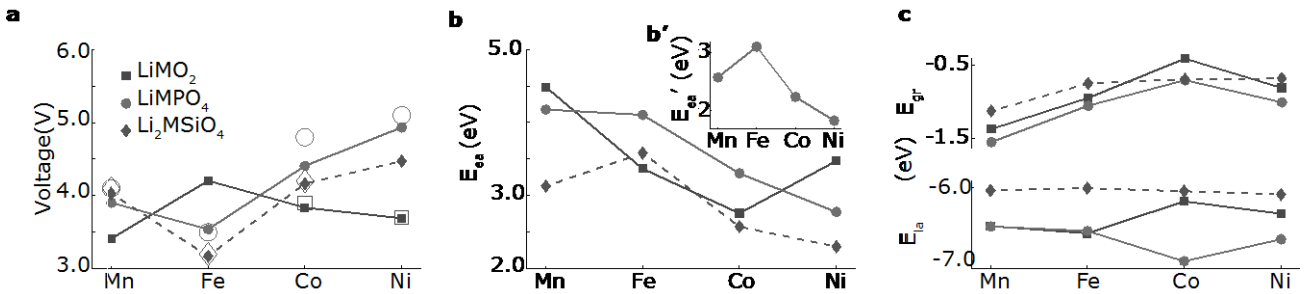

Figure 1. The voltage and energy terms. (a) Calculated and experimental values of voltage. The experimental open circuit voltage values are shown with hollow symbols excluding for $LiMnO_2$, $LiFeO_2$ and Li_2NiSiO_4, for which the experimental values are not available; (b) E_{ea}; (c) E_{la} and E_{gr}, where the upper axis is E_{gr} and the lower E_{la}. The inset of b shows the E_{ea}' values calculated based on the structures of lithiated phases of $LiMPO_4$. For Li_2MSiO_4, the redox is between Li_2MSiO_4 and $LiMSiO_4$.

PCCP RSCPublishing

ARTICLE

3 Results and discussions

3.1 Relation between charge intercalation and intercalation potential

Figure 1 shows results of the benchmark calculations of intercalation potentials and the three energy terms for three families of TME cathode materials, layered oxides ($R\bar{3}m$) $LiMO_2$, olivine phosphates (Pnma) $LiMPO_4$, and orthogonal silicates ($Pmn2_1$) Li_2MSiO_4, where M=Mn, Fe, Co, Ni. The calculated intercalation potentials agree well with experiments and other first-principles calculations.[15, 31, 32]

The term E_{ea} in Fig. 1b span wide ranges of distribution of ca. 2.1 eV, 1.5 eV, and 1.9 eV, for the oxides, phosphates, and silicates, respectively. The trend of E_{ea} with respect to TMEs exhibit a V-shape in layered oxides and a Λ-shape in both phosphates and silicates. The exact values are materials dependent, but the evolution trend approximately mirrors that of the intercalation potentials with two exceptions.One exception is $LiCoO_2$, for which both the potential and the EA are lower than $LiFeO_2$ against the mirror relation. That is due to that the expansion of the intercalation slab by Li^+ insertion is relatively smaller (the related structural information seen in Table S1) and then both the absolute values of E_{la} and E_{gr} are much larger in $LiCoO_2$ than in other $LiMO_2$ (M=Mn, Fe, Ni) materials. Another exception is $LiMnPO_4$, for which the large Jahn-Teller distortion of the coordination octahedron stabilizes the Mn^{3+}:$3d^4$ configuration in $MnPO_4$. This introduces additional Jahn-Teller splitting contribution to the EA because the intercalated electron occupies the higher e_g-level. The mirror relation between the intercalation potential and E_{ea}', calculated based on the lithiated structures of $LiMPO_4$ excluding Jahn-Teller effect, remains valid (c.f. insert Fig. 1b'). For the $LiMO_2$ series, there are two maxima of E_{ea} locating at Mn and Ni, because the E_{ea} value of CrO_2 is about 1.5 eV lower than MnO_2 and that of CuO_2 is about 1.1 eV lower than NiO_2. For both $LiMPO_4$ and Li_2MSiO_4, the maximum of E_{ea} locates at Fe. On the contrary, both E_{la} and E_{gr} are trendless with TMEs and remain in a narrower range, especially for Li_2MSiO_4, of ca. 0.1 eV and 0.4 eV, respectively, as seen in Fig. 1c.

The locations of the maxima and the evolution of E_{ea} with the TMEs is determined by the d-electron configurations. The d-electron configuration is a result of the coordination polyhedron surrounding the M cations and, to a first approximation within CF theory, depends on the competition between the mean spin-paring energy Π and the CF splitting energy △.[33] The oxygen anions form octahedra[4] and the fivefold degenerate d-levels split into two subsets of three low-lying t_{2g} and two high-lying e_g levels in $LiMO_2$ and $LiMPO_4$; whereas the ligands form tetrahedra[32] and the d-levels split into two low-lying e and three high-lying t_2 levels in Li_2MSiO_4. In $LiMO_2$, Mn and Fe ions favour high spin (HS) states whereas Co and Ni favour low spin (LS) states. For the maxima of the E_{ea}, the alternations of the d-electron configurations in electron reduction are from Mn^{4+}:$3d^3$: $t_{2g}^3 e_g^0$ to Mn^{3+}: $3d^4$: $t_{2g}^3 e_g^1$ and Ni^{4+}: $3d^6$: $t_{2g}^6 e_g^0$ to Ni^{3+}: $3d^7$: $t_{2g}^6 e_g^1$. In the phosphates and silicates, all M cations favour the HS states except for Ni^{3+} in $NiPO_4$. The reductions corresponding to the maxima of E_{ea} are from Fe^{3+}:$3d^5$: $t_{2g}^3 e_g^2$ to Fe^{2+}:$3d^6$: $t_{2g}^4 e_g^2$ and Fe^{3+}:$3d^5$: $e^2 t_2^3$ to Fe^{2+}:$3d^6$: $e^3 t_2^3$. The maxima of E_{ea} are located at cations in fully- or half-filled shell states, i.e., Mn^{4+}:$3d^3$ with the t_{2g}-subset half-filled, Ni^{4+}:$3d^6$ with the t_{2g}-subset fully-filled and Fe^{3+}:$3d^5$ with the d-shell half-filled.

3.2 Model Hamiltonian for the EA

To address the quantitative relations between the EA and the d-electron configurations, a local Hubbard model is developed within CF theory. In this model, our focus is on the d-electron localization, not on p-d bonding. Within tight-binding model, the former corresponds to the diagonal interaction in d-blocks, while the latter the off-diagonal interaction between d- and p-blocks. The interaction between the cations and the ligands is approximated by ionic interaction. We assume the d-orbital occupation is integer and the intercalated electrons are completely localized on the d-orbitals of the M cations. The ligand anions are approximated as effective point charges Q_L (accounting for the shielding effects of other cations, such as P^{5+} and Si^{4+}) locating at $\mathbf{R}_L$, other off-diagonal ligand field effects are ignored in this work. Thus the energy of a d-electron in orbital α with spin σ can be described as:

$$H = -\frac{Z^*}{\boldsymbol{r}} n_{\alpha\sigma} + \sum_L \frac{Q_L}{\boldsymbol{r} - \boldsymbol{R}_L} n_{\alpha\sigma} + \frac{1}{2} \sum_{\beta\sigma' \neq \alpha\sigma} U_{\alpha\beta} n_{\alpha\sigma} n_{\beta\sigma'} - \frac{1}{2} J_H \sum_{\beta \neq \alpha} \boldsymbol{S}_{\alpha\sigma} \boldsymbol{S}_{\beta\sigma}. \quad (1)$$

Here, the first term describes the Coulomb attraction of the effective core of the M cation and the second term the Coulomb repulsion by the ligand anions. The third and fourth terms are the on-site Coulomb and exchange interactions between the d-electrons, respectively. The α and β represent orbital, σ and σ' spin direction, n orbital occupancy, U and J_H the on-site Coulomb interaction and exchange interaction, **S** spin vector. By assuming that the CF splitting, the on-site Coulomb and exchange interaction parameters remain the same as M^{V+} is reduced to $M^{(V-1)+}$, the energy contribution of the d-electron to the EA can be estimated as

$$E_{ea}^{\alpha\sigma} \approx \{\varepsilon_d + N_d U_d\} + \left\{ f_\alpha - J_H \sum_{\beta\neq\alpha} (\boldsymbol{S}_{\alpha\sigma}\boldsymbol{S}_{\beta\sigma} - 2n_\alpha) \right\}. \quad (2)$$

Here ε_d represents the average d-level energy in the CF theory and f_α is the relative orbital energy by CF splitting, which is $-2/5\triangle_o$ for t_{2g} orbitals and $3/5\triangle_o$ for e_g in octahedral fields and $-3/5\triangle_t$ for e and $2/5\triangle_t$ for t_2 in tetrahedral fields. N_d and n_α are the d-electron number and the orbital occupancy of orbital α before the reduction, respectively. U_d is the on-site inter-orbital Coulomb repulsion parameter and the intra-orbital repulsion is chosen as U_d+2J_H.[33, 34] The two terms in the first bracket describe the average Coulomb energy cost by the reduction. The terms in the second bracket containing the contributions from CF splitting, on-site exchange interactions and the additional Coulomb repulsion between intra-orbital d-electrons referenced to inter-orbital d-electrons, i.e., $2n_\alpha J_H$ term in Eq. (3), are combined to one term named as E_{SE}, namely,

$$E_{SE} \equiv f_\alpha - J_H \sum_{\beta\neq\alpha} (\boldsymbol{S}_{\alpha\sigma}\boldsymbol{S}_{\beta\sigma} - 2n_\alpha). \quad (3)$$

E_{SE} term is susceptible to d-electron configurations and the parameterized estimations are listed in Table 1.

As seen in Table I, the contributions to E_{SE} from CF splitting term in $LiMO_2$ are positive for M=Mn, Fe, Ni, but negative for Co. The decrease in energy from the on-site exchange term is the largest for Fe. In $LiMPO_4$, the contributions to E_{SE} from CF splitting term are positive for Mn and Ni but negative for Fe and Co, and the energy decrease from the on-site exchange are larger for Mn and Ni than Co and Fe. In addition, because the d-electron number of cations HS Fe^{3+} and HS Co^{3+} are over five, the intercalated electrons have to occupy half-filled orbital and additional energy costs from the additional Coulomb repulsion are introduced. This is different from cations HS Mn^{3+} and LS Ni^{3+} in MPO_4 and all M^{4+} cations in layered MO_2, in which the intercalated electrons occupy empty orbitals. In Li_2MSiO_4, the contributions to E_{SE} from CF splitting term are positive for Mn and Ni and negative for Fe and Co, and the decrease in energy from the on-site exchange are largest for Mn and smallest for Fe. Because the intercalated electrons have to occupy the half-filled orbitals, then the reductions have to overcome the additional energy cost by the on-site intra-orbital repulsion for all M^{3+} cations except for Mn^{3+}.

Table 1 Electron configurations (E.C) alternations and the parameterized expressions of the E_{SE} term with CF splitting energies (Δ_o, Δ_t) and exchange parameters (J_H) for the three categories of cathode compounds.

$LiMO_2$			$LiMPO_4$			Li_2MSiO_4		
reduction	E.C alternation	E_{SE}	reduction	E.C alternation	E_{SE}	reduction	E.C alternation	E_{SE}
Mn^{4+} to Mn^{3+}	$t_{2g}^3e_g^0$ to $t_{2g}^3e_g^1$	$0.6\triangle_O$-$3J_H$	Mn^{3+} to Mn^{2+}	$t_{2g}^3e_g^1$ to $t_{2g}^3e_g^2$	$0.6\triangle_O$-$4J_H$	Mn^{3+} to Mn^{2+}	$e^2t_2^2$ to $e^2t_2^3$	$0.4\triangle_t$-$4J_H$
Fe^{4+} to Fe^{3+}	$t_{2g}^3e_g^1$ to $t_{2g}^3e_g^2$	$0.6\triangle_O$-$4J_H$	Fe^{3+} to Fe^{2+}	$t_{2g}^3e_g^2$ to $t_{2g}^4e_g^2$	$-0.4\triangle_O$+$2J_H$	Fe^{3+} to Fe^{2+}	$e^2t_2^3$ to $e^3t_2^3$	$-0.6\triangle_t$+$2J_H$
Co^{4+} to Co^{3+}	$t_{2g}^5e_g^0$ to $t_{2g}^6e_g^0$	$-0.4\triangle_O$	Co^{3+} to Co^{2+}	$t_{2g}^4e_g^2$ to $t_{2g}^5e_g^2$	$-0.4\triangle_O$+J_H	Co^{3+} to Co^{2+}	$e^3t_2^3$ to $e^4t_2^3$	$-0.6\triangle_t$+J_H
Ni^{4+} to Ni^{3+}	$t_{2g}^6e_g^0$ to $t_{2g}^6e_g^1$	$0.6\triangle_O$-$3J_H$	Ni^{3+} to Ni^{2+}	$t_{2g}^6e_g^1$ to $t_{2g}^6e_g^2$	$0.6\triangle_O$-$4J_H$	Ni^{3+} to Ni^{2+}	$e^4t_2^3$ to $e^4t_2^4$	$0.4\triangle_t$

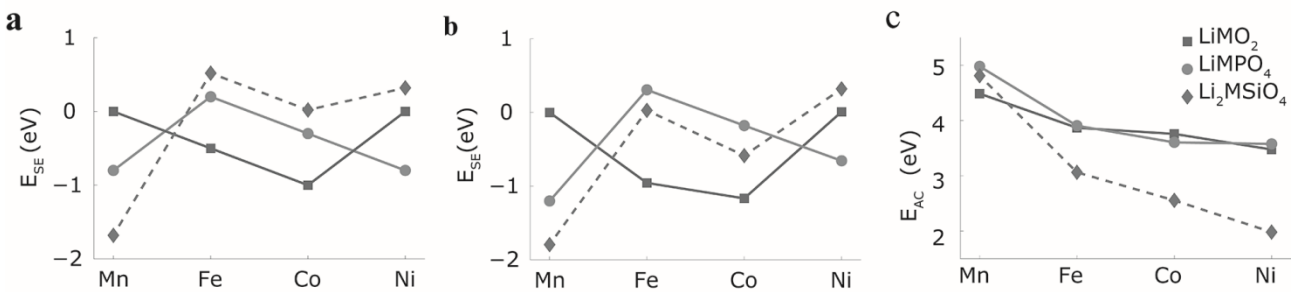

Figure 2 Energy terms E_{SE} and E_{AC}. E_{SE} are estimated with CF splitting parameters in (**a**) chosen independent of M elements as 2.5 eV, 2.0 eV, and 0.8 eV for the delithiated phases of layered oxides, phosphates, and silicates, respectively and in (**b**) derived from first-principles E_{HS}-E_{LS} energy term. (**c**) E_{AC}, the difference between E_{ea} and E_{SE} shown in (**b**).

The evolutions of the term E_{SE} are quite similar to E_{ea} except for Li_2NiSiO_4 regardless of whether the CF splitting values (Δ) is chosen as fixed for all M cations in the same structure (c.f. Fig. 2a), or approximately estimated from the first-principles energy difference between HS and LS states of the delithiated phases (c.f. Fig. 2b and the corresponding data of the energy difference between HS and LS states, and Δ are shown in Table S2). This suggests that the combination of the CF splitting and the exchange interactions dominate the trend of E_{ea} regardless of the differences in CF splitting between the M cations. Thus illustrations with the CF splitting parameter fixed for all M cations in the same structure are adopted in the future discussion for simplicity.

The remaining contributions to E_{ea}, excluding the term E_{SE}, and named here as E_{AC}, i.e.,

$$E_{AC} \equiv E_{ea} - E_{SE}, \quad (4)$$

is attributed to the two terms in the first bracket in Eq. (2) and other contributions omitted in Eq. (2), such as the d-p overlap integral and the energy promotion of the sp electrons. The contribution of d-d repulsion N_dU_d increases with the d-electron number. But, it is very interesting that E_{AC} exhibits a decreasing trend with TMEs, e.g., the value of Ni^{4+} is ca. 1.0 eV smaller than Mn^{4+} in layered oxides, as shown in Fig. 2c. This indicates that the difference in d-d Coulomb interaction energies among TMEs is totally compensated by other contributions. In addition, E_{AC} decreases with the valence state, e.g., the value of Ni^{4+} is ca. 1.4 eV smaller than Ni^{3+} in layered oxide when the energy gain from structure relaxation for Ni^{3+} relative to Ni^{4+} is omitted.

3.3 Charge order in multi-TME solid-solution composites

Charge disproportion or Jahn-Teller distortion, usually considered harmful to the electrochemical stability and/or structural stability,[35-37] occurs for the TME cations in octahedral field with d-electron configurations $t_{2g}^3e_g^1$ or $t_{2g}^6e_g^1$, e.g., HS Mn^{3+} and Fe^{4+} and LS Ni^{3+}. To exclude cations with these configurations in the fully-lithiated phase or totally-delithiated phase, solid-solutions with cations in higher or lower valence state, respectively, could be used to modify the redox activity of these TMEs, changing the redox couple from M^{3+}/M^{4+} or M^{2+}/M^{3+} to M^{2+}/M^{4+}. If TME cations M1 and M2 are solid-solutioned, charge order of the cation pair ($M1^{2+}$-$M2^{4+}$) could realize an active redox mechanism. Cation pairs ($M1^{2+}$-$M2^{4+}$) with charge order and ($M1^{3+}$-$M2^{3+}$) without charge order both can be approximately regarded as reduced from ($M1^{4+}$-$M2^{4+}$) by $2e^-$, but in different ways, i.e., from $M1^{4+}$ to $M1^{2+}$ (can be regarded as reduction from $M1^{4+}$ to $M1^{3+}$ followed by reduction $M1^{3+}$ to $M1^{2+}$), or from $M2^{4+}$ to $M2^{3+}$ together with $M1^{4+}$ to $M1^{3+}$, respectively. In the former one, only M1 is active, whereas both M1 and M2 are active in the latter one. The sub-process $M1^{4+}$ to $M1^{3+}$ is the same in both, and the only difference is in the sub-process, either from $M1^{3+}$ to $M1^{2+}$ in the former one or from $M2^{4+}$ to $M2^{3+}$ for the latter one. Then, the tendency to form an active cation pair can be judged from the energy difference in EA between the two sub-processes, defined as $\triangle E_{CO}$, which could be approximately derived as:

$$\Delta E_{CO} \approx E_{ea}(M1^{3+}) - E_{ea}(M2^{4+})$$
$$\approx \{E_{ea}(M1^{3+}) - E_{ea}(M1^{4+})\} + \{E_{ea}(M1^{4+}) - E_{ea}(M2^{4+})\}. \quad (5)$$

To generate a charge order, the value of $\triangle E_{CO}$ should be negative. Because the EA value of M^{3+} is not less than M^{4+}, to generate the charge order between M1 and M2 cations, the necessary condition from Eq. (5) is that the EA value of $M1^{4+}$ should be less than $M2^{4+}$. Thus, it is impossible to generate ($M1^{2+}$, Fe^{4+}) or ($M1^{2+}$, Co^{4+}) cation pairs at least in the layered structures, where M1 is Ni or Mn. By decomposing the E_{ea} into E_{SE} and E_{AC}, Eq. (5) can be further written as:

$$\Delta E_{CO} \approx \{E_{AC}(M1^{3+}) - E_{AC}(M1^{4+})\} - \{E_{AC}(M2^{4+}) - E_{AC}(M1^{4+})\}$$
$$+ \{E_{SE}(M1^{3+}) - E_{SE}(M1^{4+})\} - \{E_{SE}(M2^{4+}) - E_{SE}(M1^{4+})\}. \quad (6)$$

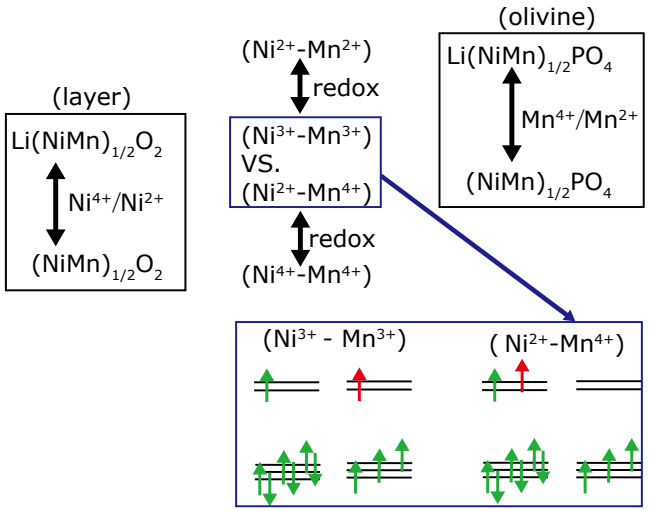

Fig.3 Redox of cation pairs in (Ni-Mn) solid-solution layered oxides and olivine phosphates, and schematic electronic level diagrams of the cation pair with or without charge order.

Interestingly, the (Ni^{2+}-Mn^{4+}) cation pair forms in the lithiated phases of layered $Li(NiMn)_{1/2}O_2$ and spinel $LiNi_{1/2}Mn_{3/2}O_4$, and the delithiated phase of $Li(NiMn)_{1/2}PO_4$, as illustrated in Fig. 3. This is by virtue of more energy gain, about $-J_H$, in the energy term E_{SE} of Ni^{3+} than in Ni^{4+}, overcoming the difference in E_{AC} between Ni^{3+} and Mn^{4+}, whereas the value of E_{SE} for Ni^{4+} is very close to Mn^{4+} (c.f. Eq. (6)). In the layered and spinel oxides, Mn is inactive and the redox couple is Ni^{2+}/Ni^{4+}.[38, 39, 40] Whereas in the redox process of $Li(NiMn)_{1/2}PO_4/(NiMn)_{1/2}PO_4$, Ni is inactive and the redox couple is Mn^{2+}/Mn^{4+}. This change in redox activity has not been recognized in previous work but it is clearly evident from in situ Ni K-edge XANES spectra that remain unchanged during the charging process up to the whole theoretical capacity of $Li(MnFeCoNi)_{1/4}PO_4$.[41] If M2 is chosen as Ti, the (Ni^{2+}-Ti^{4+}) cation pair could also form as in layered $Li(NiTi)_{1/2}O_2$,[42] due to the large difference in the E_{AC} between Ni^{4+} and Ti^{4+}.

3.4 Design of two electron redox steps

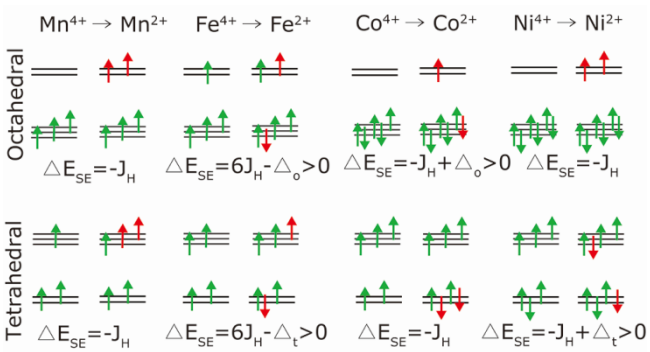

Figure 4. Schematic electronic level diagrams of the electron configuration change due to reduction with two electrons in octahedral field and tetrahedral field. $\triangle E_{SE}$ is the energy change in E_{SE} of the reduction of M^{4+} to M^{3+} relative to M^{3+} to M^{2+}.

Multi-electron redox, such as two-electron redox, opens a promising avenue to dramatically increased capacity. To be compatible with practical performance, consecutive redox plateaus are desirable. That calls for small difference in EA value among the reduction steps. For two-electron reduction, the difference in EA value between the two reduction steps, $M^{(V-1)+}$ to $M^{(V-2)+}$ and M^{V+} to $M^{(V-1)+}$, can be written as:

$$\Delta E_{ea}(M^{(V-1)+}, M^{V+}) \approx \Delta E_{AC}(M^{(V-1)+}, M^{V+}) + \Delta E_{SE}(M^{(V-1)+}, M^{V+}). \quad (7)$$

Since the E_{AC} value of $M^{(V-1)+}$ is larger than M^{V+}, to achieve redox plateaus with close voltage values, the E_{SE} value of $M^{(V-1)+}$ is preferred to be less than M^{V+}. That can only be achieved when the two intercalated electrons occupy the same subset of d-levels. For example, the redox Ni^{4+}/Ni^{2+} and Mn^{4+}/Mn^{2+} in octahedra, and Co^{4+}/Co^{2+} and Mn^{4+}/Mn^{2+} in tetrahedra can match this criterion, whereas Co^{4+}/Co^{2+} and Fe^{4+}/Fe^{2+} in octahedra, Ni^{4+}/Ni^{2+} and Fe^{4+}/Fe^{2+} in tetrahedra cannot fit in this requirement, as seen in Fig. 4. That prediction, consistent with calculations of average voltages for the latter but not for the former, agrees well with the experimental voltage profiles. Two paradigms are the layered $Li(NiMn)_{1/2}O_2$ with consecutive redox and the orthogonal Li_2FeSiO_4 with two largely separate plateaus. Further clarification on the discrepancy between our model and the routine average voltage calculations needs more detailed consideration due to dependencies on materials.

Conclusions

In the present work, we explored the role of the d-electron localization in the electron intercalation of LIB cathode compounds by developing a local Hubbard model within CF theory, combined with first-principles calculations of three types of cathodes. We found that the evolution of electron affinity with TMEs, which approximately mirrors the intercalation potential, is tightly correlated with the d-electron configuration and dominated by the combination of the CF splitting and the on-site exchange interactions. This makes new structural systems of cathode materials could be evaluated through fundamental considerations of the d-electron configurations of the redox couples. Furthermore, a concise picture of d-electron configuration alternation enables the straightforward prediction of charge order to achieve synergistic effects in multi-TME solid-solution composites and consecutive redox plateaus by two electron redox processes. The rules and principles revealed for LIB could also be extended to Na-ion battery and Mg-ion battery since the electron intercalation is mainly involved with the redox of the TMEs whereas the ion intercalation the bonding between the anion in the host and the intercalated ion.

Acknowledgements

The work was supported by programs of the Ningbo Key Innovation Team (2011B82005), the National Research program of China (2012CB722700 and 2013AA050901), the National Natural Science Foundation of China (11174301, 21303235), the National Science Foundation for Post-doctoral Scientists of China (No. 2012M521206), and the Preferred Post-doctoral Program of Zhejiang province (No. Bsh1202033). Z. Z acknowledges the NNIN program for support and resources.

Notes

a Ningbo Institute of Material Technology and Engineering, Chinese Academy of Sciences, Ningbo 315201, PR China. Fax: 086-0574-86685043; Tel: 086-0574-86688074;
b College of Physics and Information Engineering, Fuzhou University, Fuzhou 350116, PR China;
c Stanford Research Computing Facility, Stanford University, 255 Panama Street, Stanford, California 94305, USA.

Electronic Supplementary Information (ESI) available: The schematic processes deriving the three energy terms, the information of bond lengths in layered cathodes, and the CF splitting values derived from the energy difference between HS and LS states. See DOI: 10.1039/b000000x/

References

1. M. M. Thackeray, C. Wolverton and E. D. Isaacs, *Energy & Environmental Science*, 2012, **5**, 7854-7863.
2. K. Zaghib, A. Mauger, H. Groult, J. B. Goodenough and C. M. Julien, *Materials*, 2013, **6**, 1028-1049.
3. J. B. Goodenough and K.-S. Park, *Journal of the American Chemical Society*, 2013, **135**, 1167-1176.
4. A. K. Padhi, K. S. Nanjundaswamy and J. B. Goodenough, *Journal of The Electrochemical Society*, 1997, **144**, 1188-1194.
5. Z. Chen, J. Li and Z. Zhang, *Journal of Materials Chemistry*, 2012, **22**, 18968-18974.
6. J. B. Goodenough and Y. Kim, *Chemistry of Materials*, 2009, **22**, 587-603.
7. A. M. J.B. Goodenough, A.C.W.P. James and P. Strobel. , *MRS Proceedings*, 1988, **135**, 391
8. H. Chen, G. Hautier and G. Ceder, *Journal of the American Chemical Society*, 2012, **134**, 19619-19627.
9. G. Hautier, A. Jain, T. Mueller, C. Moore, S. P. Ong and G. Ceder, *Chemistry of Materials*, 2013, **25**, 2064-2074.
10. S. Curtarolo, G. L. W. Hart, M. B. Nardelli, N. Mingo, S. Sanvito and O. Levy, *Nat Mater*, 2013, **12**, 191-201.
11. F. Zhou, K. Kang, T. Maxisch, G. Ceder and D. Morgan, *Solid State Communications*, 2004, **132**, 181-186.
12. S. Q. Wu, Z. Z. Zhu, Y. Yang and Z. F. Hou, *Computational Materials Science*, 2009, **44**, 1243-1251.
13. S. Li and Z. Q. Yang, *Eur. Phys. J. B*, 2010, **78**, 299-304.
14. B. Xu and S. Meng, *Journal of Power Sources*, 2010, **195**, 4971-4976.
15. F. Zhou, M. Cococcioni, C. A. Marianetti, D. Morgan and G. Ceder, *Physical Review B*, 2004, **70**, 235121.
16. M. K. Kinyanjui, P. Axmann, M. Wohlfahrt-Mehrens, P. Moreau, F. Boucher and U. Kaiser, *Journal of Physics: Condensed Matter*, 2010, **22**, 275501.
17. C. M. Julien, *Materials Science and Engineering: R: Reports*, 2003, **40**, 47-102.
18. G. Kresse and J. Hafner, *Physical Review B*, 1994, **49**, 14251-14269.
19. G. Kresse and J. Furthmu¨ller, *Physical Review B*, 1996, **54**, 11169-11186.

20. P. E. Blochl, *Physical Review B*, 1994, **50**, 17953-17979.
21. G. Kresse and D. Joubert, *Physical Review B*, 1999, **59**, 1758-1775.
22. J. P. Perdew, K. Burke and M. Ernzerhof, *Physical Review Letters*, 1996, **77**, 3865.
23. A. I. Liechtenstein, V. I. Anisimov and J. Zaanen, *Physical Review B*, 1995, **52**, R5467.
24. M. Cococcioni and S. de Gironcoli, *Physical Review B*, 2005, **71**, 035105.
25. A. Saracibar, A. Van der Ven and M. E. Arroyo-de Dompablo, *Chemistry of Materials*, 2012, **24**, 495-503.
26. T. Ohzuku, A. Ueda, M. Nagayama, Y. Iwakoshi and H. Komori, *Electrochimica Acta*, 1993, **38**, 1159-1167.
27. A. Yamada, S. C. Chung and K. Hinokuma, *Journal of The Electrochemical Society*, 2001, **148**, A224-A229.
28. A. Nytén, A. Abouimrane, M. Armand, T. Gustafsson and J. O. Thomas, *Electrochemistry Communications*, 2005, **7**, 156-160.
29. C. Freysoldt, B. Grabowski, T. Hickel, J. Neugebauer, G. Kresse, A. Janotti and C. G. Van de Walle, *Reviews of Modern Physics*, 2014, **86**, 253-305.
30. G. Makov and M. C. Payne, *Physical Review B*, 1995, **51**, 4014-4022.
31. Z. Gong and Y. Yang, *Energy & Environmental Science*, 2011, **4**.
32. M. S. Islam, R. Dominko, C. Masquelier, C. Sirisopanaporn, A. R. Armstrong and P. G. Bruce, *Journal of Materials Chemistry*, 2011, **21**, 9811-9818.
33. L. E. Orgel, *Electronic Structures of Transition-Metal Complexes*, AIP1955.
34. P. Werner and A. J. Millis, *Physical Review Letters*, 2007, **99**, 126405.
35. M. Takano, N. Nakanishi, Y. Takeda, S. Naka and T. Takada, *Materials Research Bulletin*, 1977, **12**, 923-928.
36. Y. Shin and A. Manthiram, *Journal of The Electrochemical Society*, 2004, **151**, A204-A208.
37. I. I. Mazin, D. I. Khomskii, R. Lengsdorf, J. A. Alonso, W. G. Marshall, R. M. Ibberson, A. Podlesnyak, M. J. Martínez-Lope and M. M. Abd-Elmeguid, *Physical Review Letters*, 2007, **98**, 176406.
38. J. Reed and G. Ceder, *Electrochemical and Solid-State Letters*, 2002, **5**, A145-A148.
39. N. Yabuuchi and T. Ohzuku, *Journal of Power Sources*, 2003, **119-121**, 171-174.
40. E. Lee and K. A. Persson, *Energy & Environmental Science*, 2012, **5**, 6047-6051.
41. K.-W. Nam, X.-J. Wang, W.-S. Yoon, H. Li, X. Huang, O. Haas, J. Bai and X.-Q. Yang, *Electrochemistry Communications*, 2009, **11**, 913-916.
42. K. Kang, D. Carlier, J. Reed, E. M. Arroyo, G. Ceder, L. Croguennec and C. Delmas, *Chemistry of Materials*, 2003, **15**, 4503-4507.